Betatron Cooling of Electrons in Martian Magnetotail

Z. Z. Guo, H. S. Fu, J. B. Cao, K. Fan, Z. H. Yao, Y. Y. Liu, Z. Z. Chen, Z. Wang, X. Y. Liu, Y. Xu, et al.

Geophysical Research Letters

RESEARCH LETTER
10.1029/2021GL093826

Key Points:

- We provide the first evidence of electron betatron cooling in Martian magnetotail
- We quantitatively reproduce this cooling process by using an analytical model
- The cooling factor derived from the model agrees very well with the observation

Correspondence to:
H. S. Fu,
huishanf@gmail.com

Citation:
Guo, Z. Z., Fu, H. S., Cao, J. B., Fan, K., Yao, Z. H., Liu, Y. Y., et al. (2021). Betatron cooling of electrons in Martian magnetotail. *Geophysical Research Letters*, *48*, e2021GL093826. https://doi.org/10.1029/2021GL093826

Received 14 APR 2021
Accepted 14 JUN 2021

Betatron Cooling of Electrons in Martian Magnetotail

Z. Z. Guo[1,2], H. S. Fu[1,2], J. B. Cao[1,2], K. Fan[3], Z. H. Yao[3], Y. Y. Liu[1,2], Z. Z. Chen[1,2], Z. Wang[1,2], X. Y. Liu[1,2], Y. Xu[1,2], C. Mazelle[4], and D. L. Mitchell[5]

[1]School of Space and Environment, Beihang University, Beijing, China, [2]Key Laboratory of Space Environment Monitoring and Information Processing, Ministry of Industry and Information Technology, Beijing, China, [3]Key Laboratory of Earth and Planetary Physics, Institute of Geology and Geophysics, Chinese Academy of Sciences, Beijing, China, [4]IRAP, CNRS, University of Toulouse, UPS, CNES, Toulouse, France, [5]Space Science Laboratory, University of California, Berkeley, CA, USA

Abstract Betatron cooling, a plasma process losing particle energy in the perpendicular direction but reserving particle energy in the field-aligned direction, is a consequence of magnetic depression under the conservation of magnetic moment. Such process has been widely studied in the Earth's magnetosphere but has never been reported in other planetary environment. Here, by utilizing the Mars Atmosphere and Volatile EvolutioN (MAVEN) measurements, we report two events of betatron cooling in the Martian magnetotail. In one of the events, betatron cooling occurs in the suprathermal and energetic ranges of electrons, whereas in the other event, it occurs in the thermal-energy range. We quantitatively reproduce these two processes by using an analytical model. Gratifyingly, the cooling factor derived from the analytical model agrees well with the observation of magnetic depression. These results, for the first time demonstrating the betatron-cooling effect beyond the Earth, are useful to understand the electron dynamics in the planetary magnetosphere.

Plain Language Summary Under conservation of the magnetic moment, electrons can lose energy in the perpendicular direction but reserve energy in the field-aligned direction when magnetic field strength becomes weaker. Such process, called betatron cooling, has not been reported in the extraterrestrial planetary environment. Using the Mars Atmosphere and Volatile EvolutioN (MAVEN) data and an analytical model, for the first time, we quantitatively demonstrate and reproduce this cooling process of electrons in the Martian magnetotail, and the cooling factor derived from the analytical model agrees well with the observation. Our study promotes the understanding of the electron dynamics in the planetary magnetosphere.

1. Introduction

The planetary magnetotail, consisting of a slab-like plasma sheet and a tail-like lobe, is a nature laboratory for the exploration of plasma physics. With the help of single or multispacecraft measurements, so far, there have been many interesting electron processes reported in the Earth's magnetotail, such as the Fermi acceleration (Fu et al., 2011; Li et al., 2018; Liu & Fu, 2019; Liu, Fu, Cao, Xu et al., 2017; Lu et al., 2016), betatron acceleration (Artemyev et al., 2012, 2014; Chen et al., 2019; Fu, Khotyaintsev, et al., 2013; Fu, Xu, et al., 2019; Fu, Zhao, et al., 2020; Gabrielse et al., 2016; Grigorenko et al., 2016; Liu & Fu, 2019; Xu, Fu, Liu, et al., 2018; Zhong et al., 2020), betatron cooling (Fu et al., 2012; Liu, Fu, Xu, Wang, et al., 2017; Liu et al., 2018), nonadiabatic wave-particle interaction (Fowler et al., 2018; 2020; Fu et al., 2014; Harada et al., 2016, 2019; Huang et al., 2012; Hwang et al., 2014; Malykhin et al., 2021; Zhang et al., 2018), and so on. Among these processes, the betatron cooling of electrons is a very interesting one, as it causes electron-energy loss in the perpendicular direction but reserves electron energy in the parallel and anti-parallel directions. Consequently, during the betatron cooling, electron pitch angle distribution (PAD) evolves from the isotropic type, showing electron pitch angles uniformly from 0° to 180°, to the cigar type, showing electron pitch angles primarily at 0° and 180° (Fu, Grigorenko, et al., 2020; Liu, Fu, Xu, Cao, et al., 2017; Liu et al., 2020; Zhao et al., 2019).

Different from the Earth's intrinsic magnetotail, the Martian magnetotail is an induced one. It is formed due to the wrap of Martian ionosphere by the interplanetary magnetic field (IMF) (Acuña et al., 1999; Connerney et al., 2005; Fang et al., 2015). Thus, in principle, magnetic fields in the Martian magnetotail are actually

the distorted IMF. As a result, the Martian magnetotail is much smaller than the Earth's magnetotail, more dependent on the solar wind and IMF condition, and more active than the Earth's magnetotail. In such an active magnetotail, electron dynamics should be very complicated (e.g., Artemyev et al., 2017; DiBraccio et al., 2015; DiBraccio & Dann, 2017; DiBraccio & Luhmann, 2018; Grigorenko et al., 2017, 2019; Halekas et al., 2006; Harada et al., 2015, 2017; Inui et al., 2018; Luhmann et al., 2015; Ruhunusiri et al., 2016; Stergiopoulou et al., 2020). Particularly, one may wonder whether the betatron-cooling process can happen in such an active magnetotail. Although the electron betatron cooling has been widely reported in the decaying flux pileup region (Fu et al., 2012) and flow-reversal region (Liu et al., 2018) in the Earth's magnetotail, it has never been reported in the Martian magnetosphere.

Investigating the electron betatron cooling in the Martian magnetotail is very necessary, not only because it can improve our understanding of plasma physics beyond the Earth, but also because it can update our knowledge of the Martian space environment. Particularly, the betatron-cooling process can change the energy and pitch angle of energetic electrons, which are harmful to both the spacecraft and astronauts around the Mars.

Targeting these scientific objectives, we investigate the electron betatron-cooling process in the Martian magnetotail in this study. We report two events of such process and quantitatively we reproduce such process by using an analytical model.

2. Observation

The data we used are from the Mars Atmosphere and Volatile EvolutioN (MAVEN) mission (Jakosky et al., 2015). All the data used in this study are the level-2 calibrated data. Particularly, the magnetic field data from Magnetometer (MAG) (Connerney et al., 2015) and the electron data from Solar Wind Electron Analyzer instrument (SWEA) (Mitchell et al., 2016) are used. All the data are presented in Mars Solar Orbital (MSO) coordinates, in which X points from Mars toward the Sun, Y points opposite to the direction of Mars' orbital velocity component perpendicular to X, and Z completes the orthogonal coordinate set. In such coordinates, the positions of bow shock and magnetic pileup boundary can be estimated from the model of Trotignon et al. (2006), as shown in Figures 1a–1b and Figures 1f–1g as the black line (bow shock) and green line (magnetic pileup boundary), respectively.

The first event of interest was detected by MAVEN during 00:35−00:40 UT on April 15, 2015, when the spacecraft was located in the magnetotail at [−1.47 0.82 1.13] R_M (R_M is the Mars radius) in MSO coordinates (see the star in Figures 1a and 1b). Observations of the event are shown in Figures 1c–1e. Specifically, the magnitude and three components of magnetic fields (Figure 1c), the PAD of the 17–62 eV electrons (Figure 1d), and the omnidirectional differential energy fluxes (DEFs) of electrons (Figure 1e) are shown from top to bottom. As can be seen, in this event, the magnetic field is dominantly the B_x component. Before 00:37:10 UT and after 00:37:56 UT, the magnetic field is very stable with a value of |B|≈6 nT (Figure 1c). However, during 00:37:10–00:37:56 UT, MAVEN detected a depression of magnetic fields from |B|≈6 nT to |B|≈5 nT (see the gray shade in Figure 1c). Such depression has a duration of ∼46 s, much longer than the gyroperiod of the local electrons (about 0.007 s). It is probably caused by the solar wind disturbance, as the Martian magnetotail is an induced one and very dependent on the solar-wind condition, or may be related to the magnetic-hole structure, which has been widely observed in the Martian magnetosphere (e.g., Madanian et al., 2020). Outside the magnetic-depression region (hereafter MDR) (before 00:37:10 UT and after 00:37:56 UT), the electron DEF is relatively high (Figure 1e) and the electron PAD is either beam-like (before 00:37:10 UT, see Figure 1d) or isotropic (after 00:37:56 UT, see Figure 1d) (Fu, Grigorenko, et al., 2020; Liu et al., 2020). However, inside the MDR (00:37:10–00:37:56 UT), we clearly observe a drop of electron fluxes (Figure 1e, see the downward arrow) and a change of the electron PAD (Figure 1d) from beam-like/isotropic to the cigar type (The MAVEN spacecraft potential is typically ∼1 eV and should not exert any influence on this result. In other words, such phenomenon, electron fluxes drop inside the MDR, should be real, but not the instrumental noises). Interestingly, such drop of electron fluxes is mainly in the perpendicular direction (see Figure 1d). Considering that the time scale of this structure (∼46 s) is much longer than the electron gyroperiod, or in other words, the first adiabatic invariant (magnetic moment) is a constant, we can identify such electron-flux drop (in the perpendicular direction) associated with the magnetic depres-

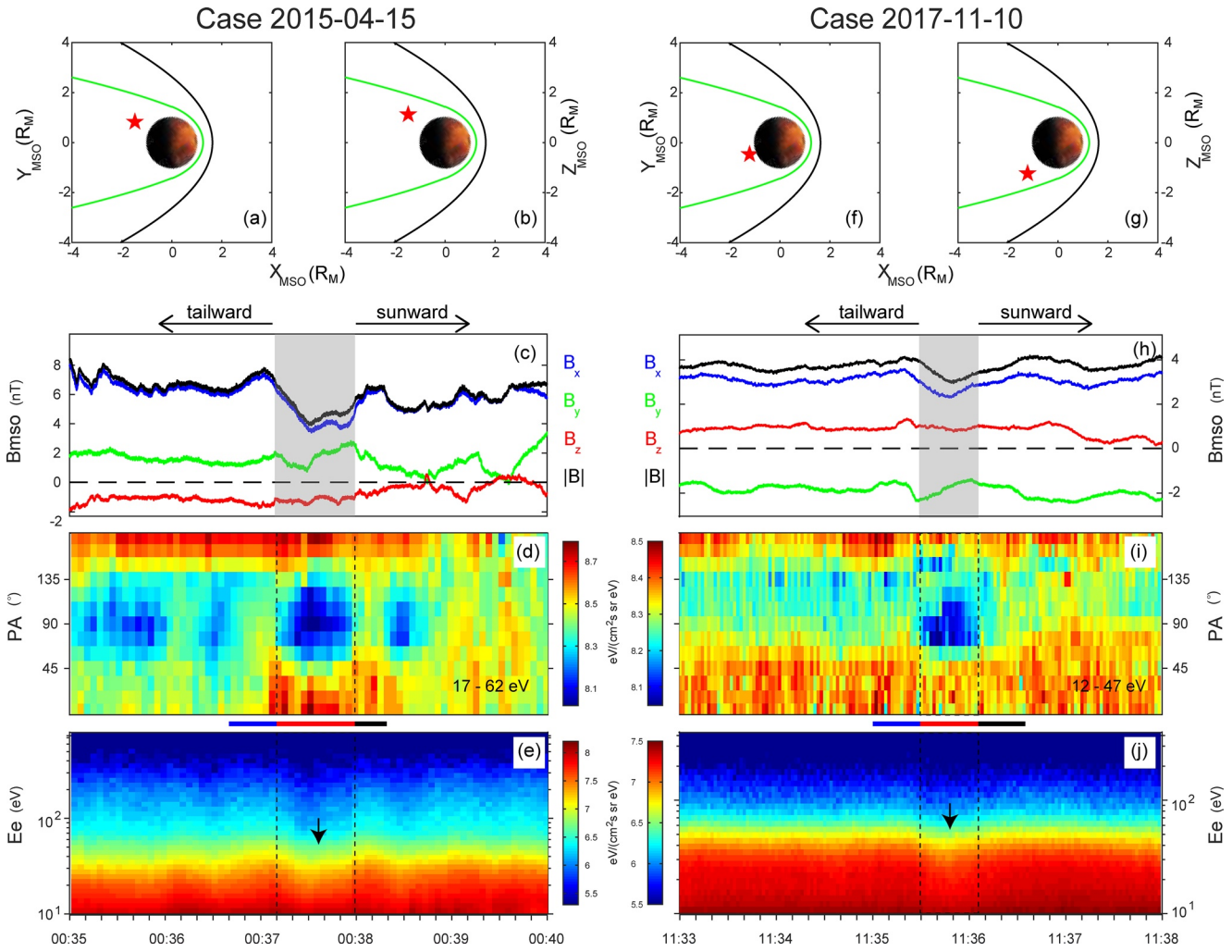

Figure 1. Overview of two events of betatron cooling measured by Mars Atmosphere and Volatile EvolutioN (MAVEN) on April 15, 2015 (left) and November 10, 2017 (right). The location of MAVEN in the X_{MSO}-Y_{MSO} plane (a, f) and in X_{MSO}-Z_{MSO} plane (b, g). The black and green lines represent the nominal positions of the bow shock and magnetic pileup boundary, respectively. MAVEN observations of (c, h) magnetic field B_x, B_y, B_z, and |B| components, (d, i) the pitch angle distribution of electrons, and (e, j) the omnidirectional differential energy fluxes of electrons. The shaded area indicates the time period of betatron cooling. MSO represents the Mars Solar Orbital coordinates.

sion as the betatron-cooling process. To our knowledge, this is the first evidence of electron betatron cooling in the Martian magnetosphere.

Interestingly, such phenomenon, electron betatron cooling, is not unique in the Martian environment. We survey the MAVEN measurements in the Martian magnetotail and find another event on November 10, 2017 at [−1.19 −0.463 −1.23] R_M (see the star in Figures 1f-1g). Figures 1h–1j are an overview of this event, in the same format as Figures 1c–1e. As can be seen, all the particle and field features in this event are quite similar to those in event 2015-04-15. Approximately, the magnetic depression (from |B|≈3.5 nT to |B|≈3 nT) is observed during 11:35:30−11:36:05 UT (see the gray shade in Figure 1h). Outside the MDR (before 11:35:30 UT and after 11:36:05 UT), the electron DEF is relatively high (Figure 1j) and the electron PAD has a weak cigar shape (Figure 1i) (Fu, Grigorenko, et al., 2020; Liu et al., 2020), whereas inside the MDR (11:35:30−11:36:05 UT), the electron DEF significantly drops (Figure 1j, see the downward arrow) and the electron PAD has a very strong cigar shape (Figure 1i). Similar as the first event, the time scale of this magnetic depression (~35 s) is much longer than the gyroperiod of local electrons (~0.009 s). Therefore, once again, we can identify the electron-flux drop in this event (associated with the magnetic depression and appearing primarily in the perpendicular direction) as the betatron-cooling process.

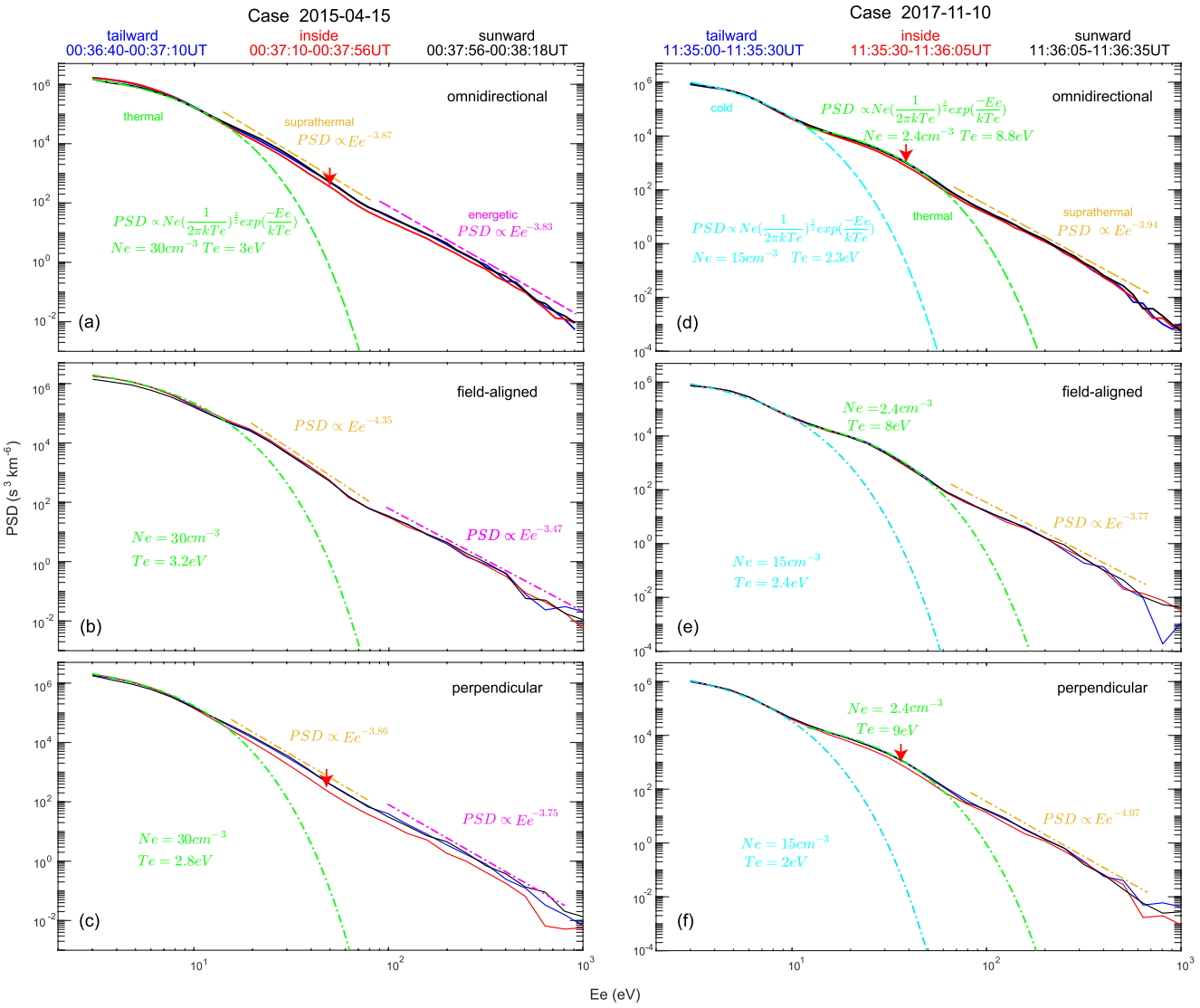

Figure 2. The electron phase space density (PSD) as a function of electron energy on April 15, 2015 (left) and November 10, 2017 (right). (a, d) The omnidirection PSD, (b, e) the field-aligned PSD, and (c, f) the perpendicular PSD as a function of electron energy inside the magnetic-depression region (MDR) (red curves) and outside the MDR (black curves and blue curves). The cyan and green dashed lines represent the Maxwellian models, for fitting cold and thermal electron distributions, respectively. The orange and purple dashed lines represent the power law models, for fitting electron distributions at suprathermal and energetic ranges, respectively. Since the PSDs outside the MDR are similar, we only fit the blue lines.

Figures 2a–2c present the electron phase space density (PSD) as a function of electron energy in three different directions (omnidirectional, field-aligned direction, and perpendicular direction) and three regions (tailward of MDR, inside the MDR, sunward of MDR), for the first event (Case 2015-04-25). Specifically, the perpendicular direction is defined as the pitch angles between 52.5° and 127.5°; the field-aligned direction is defined as the pitch angles of 0°–37.5° and 142.5°–180°; the three regions are detected at 00:36:40–00:37:10 UT (tailward of MDR, see the blue bar below Figure 1d), 00:37:10–00:37:56 UT (inside the MDR, see the red bar below Figure 1d), and 00:37:56–00:38:18 UT (sunward of MDR, see the black bar below Figure 1d). In the omnidirection (Figure 2a), we find that the electron PSDs at the tailward of MDR (blue solid line) and at the sunward of MDR (black solid line) are quite similar. We can fit these PSDs by using a Maxwellian distribution and two power-law distributions. Quantitatively, the Maxwellian distribution is $\mathrm{PSD} \propto N_e \left(1/2\pi k T_e\right)^{3/2} \exp\left(-E_e/kT_e\right)$ with $N_e = 30\mathrm{cm}^{-3}$ and $T_e = 3\,\mathrm{eV}$ (see the green dashed line in Figure 2a), which describes the 3–15 eV electrons well; the first power-law distribution is $\mathrm{PSD} \propto E_e^{-\gamma}$ with

$\gamma = 3.87$ (see the orange dashed line in Figure 2a), which describes the 15–80 eV electrons well; the second power-law distribution is PSD $\propto E_e^{-\gamma}$ with $\gamma = 3.83$ (see the purple dashed line in Figure 2a), which describes the 80–1,000 eV electrons well. In this way, we can identify the 3–15 eV electrons, 15–80 eV electrons, and 80–1,000 eV electrons in this event as the thermal, suprathermal, and energetic, respectively, following previous studies (Fu, Grigorenko, et al., 2020; Fu, Peng, et al., 2019; Zhao et al., 2019). Similarly, in the field-aligned direction (Figure 2b), we can fit the electron PSD by using the Maxwellian distribution (with parameters $N_e = 30\text{cm}^{-3}$ and $T_e = 3.2\,\text{eV}$) and the power-law distributions (with parameters $\gamma = 4.35$ and $\gamma = 3.47$); in the perpendicular direction (Figure 2c), we fit the PSD by using the Maxwellian distribution (with parameters $N_e = 30\text{cm}^{-3}$ and $T_e = 2.8\,\text{eV}$) and the power-law distributions (with parameters $\gamma = 3.86$ and $\gamma = 3.75$). Here, the thermal population may originate from the Martian ionosphere or solar wind, whereas the energetic population is probably the Solar Energetic Particles, which are very common across the whole solar system and typically have a power-law spectrum (Oka et al., 2018; Pierrard & Lazar, 2010).

As can be seen, in the field-aligned direction (Figure 2b), the electron PSDs in all three regions (tailward of MDR, inside the MDR, sunward of MDR) are almost the same. However, in the omnidirection (Figure 2a) and perpendicular direction (Figure 2c), the electron PSDs inside the MDR (red solid line) are lower than those outside the MDR (blue and black solid lines). This means that the drop of electron PSDs inside the MDR only appears in the perpendicular direction but not appears in the field-aligned direction, which is a clear signature of the betatron-cooling process (e.g., Chisham et al., 1998; Fu et al., 2012; Liu et al., 2018; Pantellini, 1998). Interestingly, such betatron cooling is most prominent in the suprathermal and energetic ranges (Figure 2a).

Using a same methodology, we analyze the second event (Case 2017-11-10). The results are presented in Figures 2d–2f, in the same format as Figures 2a–2c. Here, the three regions are at the tailward of the MDR (11:35:00–11:35:30 UT, see the blue bar below Figure 1i), inside the MDR (11:35:30–11:36:05 UT, see the red bar below Figure 1i), and at the sunward of the MDR (11:36:05–11:36:35 UT, see the black bar below Figure 1i), respectively. The definition of the field-aligned and perpendicular directions is same as that in the first event. To have the best match, here we use two Maxwellian distributions PSD $\propto N_e\left(1/2\pi kT_e\right)^{3/2}\exp\left(-E_e/kT_e\right)$ and one power-law distribution PSD $\propto E_e^{-\gamma}$ to fit the electron PSDs, and naturally we can identify the cold population (3–10 eV electrons), thermal population (10–60 eV electrons), and suprathermal population (60–1,000 eV electrons) in the event. Respectively, the fitting parameters are $N_e = 15\text{cm}^{-3}$, $T_e = 2.3\,\text{eV}$, $N_e = 2.4\text{cm}^{-3}$, $T_e = 8.8\,\text{eV}$, $\gamma = 3.94$ in the omnidirection (see Figure 2d), $N_e = 15\text{cm}^{-3}$, $T_e = 2.4\,\text{eV}$, $N_e = 2.4\text{cm}^{-3}$, $T_e = 8\,\text{eV}$, $\gamma = 3.77$ in the field-aligned direction (see Figure 2e), and $N_e = 15\text{cm}^{-3}$, $T_e = 2\,\text{eV}$, $N_e = 2.4\text{cm}^{-3}$, $T_e = 9\,\text{eV}$, $\gamma = 4.07$ in the perpendicular direction (see Figure 2f). Generally, we find a similar feature as in the first event: the electron PSDs are almost identical in all three regions (tailward of MDR, inside the MDR, sunward of MDR) in the field-aligned direction (see Figure 2e), but exhibit a clear drop inside the MDR in both the omnidirection and perpendicular direction (see the red solid lines in Figures 2d and 2f). Apparently, this is the signature of betatron cooling. However, differing from the previous event, we find that the drop of electron PSDs in this event is most prominent in the thermal-energy range (see the downward arrows in Figures 2d and 2f). The low-energy electrons have no clear response to betatron cooling. This is probably due to the nonadiabatic interaction between low-energy electrons and waves, as suggested by Fu et al. (2011) and Liu and Fu (2019). However, such conjecture cannot be verified because the measurements of waves are unavailable in the MAVEN spacecraft.

3. Modeling of Betatron Cooling

We can reproduce such betatron-cooling process by using an analytical model based on the Liouville's theorem, as done in previous studies (e.g., Fu et al., 2011; Fu, Khotyaintsev, et al., 2013; Xu, Fu, Liu, et al., 2018). According to the analyses in Figure 2, we naturally treat the electrons outside the MDR as the source population and treat the electrons inside the MDR as the consequence population after betatron cooling. Specifically, the model is (Fu, Khotyaintsev, et al., 2013):

$$E_{1\|} = \left(L_0/L_1\right)^2 \cdot E_{0\|} = F_f \cdot E_{0\|}$$

$$E_{1\perp} = \left(B_1/B_0\right) \cdot E_{0\perp} = F_b \cdot E_{0\perp}$$

where E, L, B, F_f, and F_b represent the electron energy, the bouncing distance of electrons, the magnetic field strength, the Fermi factor, and the betatron factor, respectively; the subscripts "0" and "1" correspond to the source population and consequence population, respectively; and the symbols "⊥" and "‖" indicate the perpendicular direction and field-aligned direction, respectively. Both the betatron and Fermi effects are considered in this model. Notice that electrons with different pitch angles have different mirror points (bouncing distance): when the pitch angle is close to 0° or 180°, the bouncing distance of electrons is approximately the length of magnetic field lines; when the pitch angle is close to 90°, the bouncing distance of electrons is much shorter than the length of magnetic field lines. In other words, electrons with different pitch angles may react on the magnetic-field-line shrinking differently.

The modeling results are shown in Figure 3. For Case 2015-04-15, we use the electron population measured during 00:37:56–00:38:18 UT (outside the MDR, see the black bar below Figure 1d and black lines in Figures 2a–2c) as the source population and use the electron population measured during 00:37:10–00:37:56 UT (inside the MDR, see the red bar below Figure 1d and red lines in Figures 2a–2c) as the "consequence," and consider primarily the suprathermal and energetic electrons because the PSD evolution is most clear in this energy range (see Figures 2a and 2c). In the same way, for Case 2017-11-10, we take the electrons measured at 11:36:05–11:36:35 UT as the "source" and the electrons at 11:35:30–11:36:05 UT as the "consequence", and we consider only the thermal electrons (see Figures 2d and 2f). The modeling results are shown in Figures 3b and 3d as the dashed lines. The Fermi and betatron factors are obtained by best fitting the modeling results (dashed lines) to the MAVEN observations (solid lines). In both cases, the Fermi factor (F_f) is very close to 1, meaning that the Fermi effect does not contribute to the PSD evolution, consistent with the results in Figures 2b and 2e. However, in both cases, the betatron factor is greatly smaller than 1, indicating that the betatron effect contributes significantly to the PSD evolution. The values of betatron factor ($F_b = 0.84$ and $F_b = 0.82$) indicate weakening of magnetic fields by 17% (see the equation above). Considering that the magnetic-field strength drops by 17% in the first event (from |B|≈6 nT outside the MDR to |B|≈5 nT inside the MDR, see the black line in Figure 1c) and drops by 15% in the second event (from |B|≈3.5 nT outside the MDR to |B|≈3 nT inside the MDR, see the black line in Figure 1h), the betatron factors derived from the analytical model (Figures 3b and 3d) are very reasonable. In other words, we have quantitatively confirmed the betatron-cooling process in these two events.

The absence of Fermi acceleration/cooling in the Martin magnetotail is also reasonable. Actually, to execute such process, magnetic field lines must shrink (acceleration) or relax (cooling), which is possible in the Earth's magnetotail during the dipolarization after magnetic reconnection (Fu, Cao, et al., 2013; Xu, Fu, Norgren, et al., 2018). However, in the Martin magnetotail, the situation is a bit different: magnetic field lines are not connected to the Mars. In such situation, dipolarization process (magnetic-field-line shrinking) does not exist in the Martin magnetotail, even though magnetic reconnection can happen there (Harada et al., 2015). As a result, we cannot expect Fermi acceleration/cooling in the Martin magnetotail as in the Earth's magnetotail.

4. Conclusions and Discussion

In this letter, for the first time, we report the betatron cooling of electrons in the Martian magnetotail, by utilizing the MAVEN measurements on April 15, 2015 and November 10, 2017. Such betatron cooling is caused by the local depression of magnetic fields under the conservation of the first adiabatic invariant (magnetic moment) and leads to the drop of electron fluxes in the perpendicular direction. It significantly alters the electron PAD, and consequently affects the electron dynamics in the Martian magnetotail. We find that such betatron-cooling process can happen in the thermal-energy range (Case 2017-11-10), suprathermal -energy range (Case 2015-04-15), and energetic range (Case 2015-04-15). Quantitatively, we reproduce such betatron-cooling process by using an analytical model. In both events, the cooling factor derived from

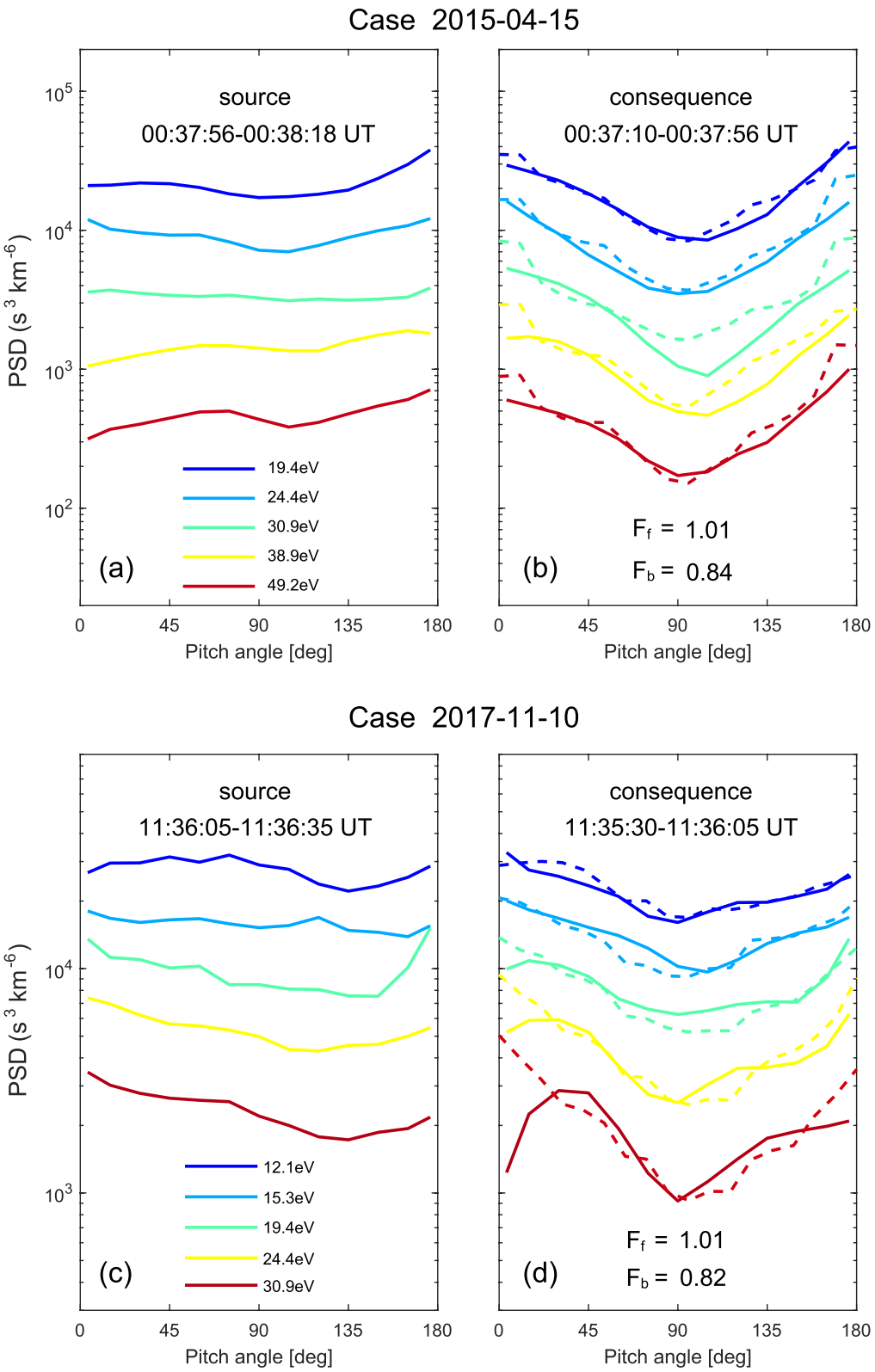

Figure 3. Phase space density (PSD) plotted as a function of pitch angle on April 15, 2015 (up) and November 10, 2017 (down). (a) PSD, after the period (00:37:56–00:38:18 UT) where betatron cooling occurs, is treated as the source. (b) PSD, during period (00:37:10–00:37:56 UT), where betatron cooling occurs, is considered to be the consequence. Solid lines represent the observations of Mars Atmosphere and Volatile EvolutioN (MAVEN), while dashed lines show the modeling results. Panels (c, d) are in the same format as Panels (a, b).

the analytical model agrees well with the MAVEN observations of magnetic depression, meaning that our modeling results are considerably reliable.

Such phenomenon, electron betatron cooling, has greatly improved our understanding of the magnetic transients and electron dynamics in the Martian magnetotail. It also has updated our knowledge of the Martian space environment, which is very useful particularly for the future spacecraft/astronauts to the Mars. Therefore, although betatron cooling of electrons has been widely reported in the Earth's magnetosphere, discovery of this process in the Martian magnetosphere is still significant. However, reporting only two events and quantitatively explaining these events are not enough. To fully understand this phenomenon, a statistical investigation, including the structure scale, occurrence rate, spatial distribution in the Martian magnetosphere, relation with the solar-wind speed, relation with the IMF condition, relation with the Martian ionosphere (or solar flare), etc., is very necessary. We will carry out such a statistical study in our future work.

Data Availability Statement

All MAVEN data are available at the Planetary Data System (https://pds-ppi.igpp.ucla.edu).

Acknowledgments
The authors appreciate the valuable suggestions from J. Cui at Sun Yat-sen University and J. E. Connerney at Goddard Space Flight Center. This work was supported by NSFC Grants 41821003 and 41874188.

References

Acuña, M., Connerney, J., Ness, N. F., Lin, R. P., Mitchell, D., Carlson, C. W., et al. (1999). Global distribution of crustal magnetization discovered by the Mars Global Surveyor MAG/ER experiment. *Science*, *284*, 790–793. https://doi.org/10.1126/science.284.5415.790

Artemyev, A. V., Angelopoulos, V., Halekas, J. S., Runov, A., Zelenyi, L. M., & McFadden, J. P. (2017). Mars's magnetotail: Nature's current sheet laboratory. *Journal of Geophysical Research: Space Physics*, *122*, 5404–5417. https://doi.org/10.1002/2017JA024078

Artemyev, A. V., Petrukovich, A. A., Nakamura, R., & Zelenyi, L. M. (2012). Adiabatic electron heating in the magnetotail current sheet: Cluster observations and analytical models. *Journal of Geophysical Research*, *117*, A06219. https://doi.org/10.1029/2012JA017513

Artemyev, A. V., Walsh, A. P., Petrukovich, A. A., Baumjohann, W., Nakamura, R., & Fazakerley, A. N. (2014). Electron pitch angle/energy distribution in the magnetotail. *Journal of Geophysical Research: Space Physics*, *119*, 7214–7227. https://doi.org/10.1002/2014JA020350

Chen, G., Fu, H. S., Zhang, Y., Li, X., Ge, Y. S., Du, A. M., et al. (2019). Energetic electron acceleration in unconfined reconnection jets. *The Astrophysical Journal Letters*, *881*, L8. https://doi.org/10.3847/2041-8213/ab3041

Chisham, G., Burgess, D., Schwartz, S. J., & Dunlop, M. W. (1998). Observations of electron distributions in magnetosheath mirror mode waves. *Journal of Geophysical Research*, *103*, 26765–26774. https://doi.org/10.1029/98JA02620

Connerney, J. E. P., Acuña, M., Ness, N., Kletetschka, G., Mitchell, D., Lin, R., & Reme, H. (2005). Tectonic implications of Mars crustal magnetism. *Proceedings of the National Academy of Sciences of the USA*, *102*, 14970–14975. https://doi.org/10.1073/pnas.0507469102

Connerney, J. E. P., Espley, J., Lawton, P., Murphy, S., Odom, J., Oliversen, R., & Sheppard, D. (2015). The MAVEN magnetic field investigation. *Space Science Reviews*, *195*, 257–291. https://doi.org/10.1007/s11214-015-0169-4

DiBraccio, G. A., Dann, J., Espley, J. R., Gruesbeck, J. R., Soobiah, Y., Connerney, J. E. P., et al. (2017). Maven observations of tail current sheet flapping at mars. *Journal of Geophysical Research: Space Physics*, *122*, 4308–4324. https://doi.org/10.1002/2016JA023488

DiBraccio, G. A., Espley, J. R., Gruesbeck, J. R., Connerney, J. E. P., Brain, D. A., Halekas, J. S., et al. (2015). Magnetotail dynamics at Mars: Initial MAVEN observations. *Geophysical Research Letters*, *42*, 8828–8837. https://doi.org/10.1002/2015GL065248

DiBraccio, G. A., Luhmann, J. G., Curry, S. M., Espley, J. R., Xu, S., Mitchell, D. L., et al. (2018). The twisted configuration of the Martian magnetotail: MAVEN observations. *Geophysical Research Letters*, *45*, 4559–4568. https://doi.org/10.1029/2018GL077251

Fang, X., Ma, Y., Brain, D., Dong, Y., & Lillis, R. (2015). Control of Mars global atmospheric loss by the continuous rotation of the crustal magnetic field: A time-dependent MHD study. *Journal of Geophysical Research: Space Physics*, *120*, 10926–10944. https://doi.org/10.1002/2015JA021605

Fowler, C. M., Agapitov, O. V., Xu, S., Mitchell, D. L., Andersson, L., Artemyev, A., et al. (2020). Localized heating of the Martian topside ionosphere through the combined effects of magnetic pumping by large-scale magnetosonic waves and pitch angle diffusion by whistler waves. *Geophysical Research Letters*, *47*, e2019GL086408. https://doi.org/10.1029/2019GL086408

Fowler, C. M., Andersson, L., Ergun, R. E., Harada, Y., Hara, T., Collinson, G., et al. (2018). MAVEN observations of solar wind-driven magnetosonic waves heating the Martian dayside ionosphere. *Journal of Geophysical Research: Space Physics*, *123*, 4129–4149. https://doi.org/10.1029/2018JA025208

Fu, H. S., Cao, J. B., Cully, C. M., Khotyaintsev, Y. V., Vaivads, A., Angelopoulos, V., et al. (2014). Whistler-mode waves inside flux pileup region: Structured or unstructured? *Journal of Geophysical Research: Space Physics*, *119*, 9089–9100. https://doi.org/10.1002/2014JA020204

Fu, H. S., Cao, J. B., Khotyaintsev, Y. V., Sitnov, M. I., Runov, A., Fu, S. Y., et al. (2013b). Dipolarization fronts as a consequence of transient reconnection: In situ evidence. *Geophysical Research Letters*, *40*, 6023–6027. https://doi.org/10.1002/2013GL058620

Fu, H. S., Grigorenko, E. E., Gabrielse, C., Liu, C., Lu, S., Hwang, K. J., et al. (2020b). Magnetotail dipolarization fronts and particle acceleration: A review. *Science China Earth Sciences*, *63*, 235–256. https://doi.org/10.1007/s11430-019-9551-y

Fu, H. S., Khotyaintsev, Y. V., André, M., & Vaivads, A. (2011). Fermi and betatron acceleration of suprathermal electrons behind dipolarization fronts. *Geophysical Research Letters*, *38*, L16104. https://doi.org/10.1029/2011GL048528

Fu, H. S., Khotyaintsev, Y. V., Vaivads, A., André, M., Sergeev, V. A., Huang, S. Y., et al. (2012). Pitch angle distribution of suprathermal electrons behind dipolarization fronts: A statistical overview. *Journal of Geophysical Research*, *117*, A12221. https://doi.org/10.1029/2012JA018141

Fu, H. S., Khotyaintsev, Y. V., Vaivads, A., Retinò, A., & André, M. (2013a). Energetic electron acceleration by unsteady magnetic reconnection. *Nature Physics*, *9*, 426–430. https://doi.org/10.1038/NPHYS2664

Fu, H. S., Peng, F. Z., Liu, C. M., Burch, J. L., Gershman, D. G., & Le Contel, O. (2019b). Evidence of electron acceleration at a reconnecting magnetopause. *Geophysical Research Letters*, *46*, 5645–5652. https://doi.org/10.1029/2019GL083032

Fu, H. S., Xu, Y., Vaivads, A., & Khotyaintsev, Y. V. (2019a). Super-efficient electron acceleration by an isolated magnetic reconnection. *The Astrophysical Journal Letters*, *870*, L22. https://doi.org/10.3847/2041-8213/aafa75

Fu, H. S., Zhao, M. J., Yu, Y., & Wang, Z. (2020a). A new theory for energetic electron generation behind dipolarization front. *Geophysical Research Letters*, *47*, e2019GL086790. https://doi.org/10.1029/2019GL086790

Gabrielse, C., Harris, C., Angelopoulos, V., Artemyev, A., & Runov, A. (2016). The role of localized inductive electric fields in electron injections around dipolarizing flux bundles. *Journal of Geophysical Research: Space Physics*, *121*, 9560–9585. https://doi.org/10.1002/2016JA023061

Grigorenko, E. E., Kronberg, E. A., Daly, P. W., Ganushkina, N. Y., Lavraud, B., Sauvaud, J.-A., & Zelenyi, L. M. (2016). Origin of low proton-to-electron temperature ratio in the Earth's plasma sheet. *Journal of Geophysical Research: Space Physics*, *121*, 9985–10004. https://doi.org/10.1002/2016JA022874

Grigorenko, E. E., Shuvalov, S. D., Malova, H. V., Dubinin, E., Popov, V. Y., Zelenyi, L. M., et al. (2017). Imprints of quasi-adiabatic ion dynamics on the current sheet structures observed in the Martian magnetotail by MAVEN. *Journal of Geophysical Research: Space Physics*, *122*, 10176–10193. https://doi.org/10.1002/2017JA024216

Grigorenko, E. E., Zelenyi, L. M., DiBraccio, G., Ermakov, V. N., Shuvalov, S. D., Malova, H. V., et al. (2019). Thin current sheets of sub-ion scales observed by MAVEN in the Martian magnetotail. *Geophysical Research Letters*, *46*, 6214–6222. https://doi.org/10.1029/2019GL082709

Halekas, J., Brain, D., Lillis, R. J., Fillingim, M. O., Mitchell, D. L., & Lin, R. P. (2006). Current sheets at low altitudes in the Martian magnetotail. *Geophysical Research Letters*, *33*, L13101. https://doi.org/10.1029/2006GL026229

Harada, Y., Andersson, L., Fowler, C. M., Mitchell, D. L., Halekas, J. S., Mazelle, C., et al. (2016). MAVEN observations of electron-induced whistler mode waves in the Martian magnetosphere. *Journal of Geophysical Research: Space Physics*, *121*, 9717–9731. https://doi.org/10.1002/2016JA023194

Harada, Y., Halekas, J. S., McFadden, J. P., Espley, J., DiBraccio, G. A., Mitchell, D. L., et al. (2017). Survey of magnetic reconnection signatures in the Martian magnetotail with MAVEN. *Journal of Geophysical Research: Space Physics*, *122*, 5114–5131. https://doi.org/10.1002/2017JA023952

Harada, Y., Halekas, J. S., McFadden, J. P., Mitchell, D. L., Mazelle, C., Connerney, J. E. P., et al. (2015). Magnetic reconnection in the near-Mars magnetotail: MAVEN observations. *Geophysical Research Letters*, *42*, 8838–8845. https://doi.org/10.1002/2015GL065004

Harada, Y., Ruhunusiri, S., Halekas, J. S., Espley, J., DiBraccio, G. A., Mcfadden, J. P., et al. (2019). Locally generated ULF waves in the Martian magnetosphere: MAVEN observations. *Journal of Geophysical Research: Space Physics*, *124*, 8707–8726. https://doi.org/10.1029/2019JA027312

Huang, S. Y., Zhou, M., Deng, X. H., Yuan, Z. G., Pang, Y., Wei, Q., et al. (2012). Kinetic structure and wave properties associated with sharp dipolarization front observed by Cluster. *Annales Geophysicae*, *30*, 97–107. https://doi.org/10.5194/angeo-30-97-2012

Hwang, K.-J., Goldstein, M. L., F-Viñas, A., Schriver, D., & Ashour-Abdalla, M. (2014). Wave-particle interactions during a dipolarization front event. *Journal of Geophysical Research: Space Physics*, *119*, 2484–2493. https://doi.org/10.1002/2013JA019259

Inui, S., Seki, K., Namekawa, T., Sakai, S., Brain, D. A., Hara, T., et al. (2018). Cold dense ion outflow observed in the Martian-induced magnetotail by MAVEN. *Geophysical Research Letters*, *45*, 5283–5289. https://doi.org/10.1029/2018GL077584

Jakosky, B. M., Lin, R. P., Grebowsky, J. M., Luhmann, J. G., Mitchell, D. F., Beutelschies, G., et al. (2015). The Mars atmosphere and volatile evolution (MAVEN) mission. *Space Science Reviews*, *195*, 3–48. https://doi.org/10.1007/s11214-015-0139-x

Li, X., Guo, F., Li, H., & Li, S. (2018). Large-scale compression acceleration during magnetic reconnection in a low-β plasma. *The Astrophysical Journal*, *866*, 4. https://doi.org/10.3847/1538-4357/aae07b

Liu, C. M., & Fu, H. S. (2019). Anchor point of electron acceleration around dipolarization fronts in space plasmas. *The Astrophysical Journal Letters*, *873*, L2. https://doi.org/10.3847/2041-8213/ab06cb

Liu, C. M., Fu, H. S., Cao, J. B., Xu, Y., Yu, Y. Q., Kronberg, E. A., & Daly, P. W. (2017a). Rapid pitch angle evolution of suprathermal electrons behind dipolarization fronts. *Geophysical Research Letters*, *44*, 10116–10124. https://doi.org/10.1002/2017GL075007

Liu, C. M., Fu, H. S., Liu, Y. Y., Wang, Z., Chen, G., Xu, Y., & Chen, Z. Z. (2020). Electron pitch-angle distribution in Earth's magnetotail: Pancake, cigar, isotropy, butterfly and rolling-pin. *Journal of Geophysical Research: Space Physics*, *125*, e2020JA027777. https://doi.org/10.1029/2020JA027777

Liu, C. M., Fu, H. S., Xu, Y., Cao, J. B., & Liu, W. L. (2017c). Explaining the rolling-pin distribution of suprathermal electrons behind dipolarization fronts. *Geophysical Research Letters*, *44*, 6492–6499. https://doi.org/10.1002/2017GL074029

Liu, C. M., Fu, H. S., Xu, Y., Wang, T. Y., Cao, J. B., Sun, X. G., & Yao, Z. H. (2017b). Suprathermal electron acceleration in the near-Earth flow rebounce region. *Journal of Geophysical Research: Space Physics*, *122*, 594–604. https://doi.org/10.1002/2016JA023437

Liu, C. M., Liu, Y. Y., Xu, Y., & Zhao, M. J. (2018). Betatron cooling of suprathermal electrons in the terrestrial magnetotail. *The Astrophysical Journal*, *866*, 93. https://doi.org/10.3847/1538-4357/aade8c

Lu, S., Angelopoulos, V., & Fu, H. (2016). Suprathermal particle energization in dipolarization fronts: Particle-in-cell simulations. *Journal of Geophysical Research: Space Physics*, *121*, 9483–9500. https://doi.org/10.1002/2016JA022815

Luhmann, J., Dong, C., Ma, Y., Curry, S. M., Mitchell, D., Espley, J., et al. (2015). Implications of MAVEN Mars near-wake measurements and models. *Geophysical Research Letters*, *42*, 9087–9094. https://doi.org/10.1002/2015GL066122

Madanian, H., Halekas, J. S., Mazelle, C. X., Omidi, N., Espley, J. R., Mitchell, D. L., & McFadden, J. P. (2020). Magnetic holes upstream of the Martian bow shock: MAVEN observations. *Journal of Geophysical Research: Space Physics*, *125*, e2019JA027198. https://doi.org/10.1029/2019JA027198

Malykhin, A. Y., Grigorenko, E. E., & Shklyar, D. R. (2021). MMS observations of narrow-band quasi-parallel whistler waves in the flow braking region in near-earth magnetotail. *Cosmic Research*, *59*, 6–14. https://doi.org/10.1134/S0010952521010044

Mitchell, D. L., Mazelle, C., Sauvaud, J.-A., Thocaven, J.-J., Rouzaud, J., Fedorov, A., et al. (2016). The MAVEN solar wind electron analyzer. *Space Science Reviews*, *200*, 495–528. https://doi.org/10.1007/s11214-015-0232-1

Oka, M., Birn, J., Battaglia, M., Chaston, C. C., Hatch, S. M., Livadiotis, G., et al. (2018). Electron Power-Law Spectra in Solar and Space Plasmas. *Space Science Reviews*, *214*, 82. https://doi.org/10.1007/s11214-018-0515-4

Pantellini, F. G. E. (1998). A model of the formation of stable non-propagating magnetic structures in the solar wind based on the nonlinear mirror instability. *Journal of Geophysical Research*, *103*, 4789–4798. https://doi.org/10.1029/97JA02384

Pierrard, V., & Lazar, M. (2010). Kappa Distributions: Theory and Applications in Space Plasmas. *Solar Physics*, *267*, 153–174. https://doi.org/10.1007/s11207-010-9640-2

Ruhunusiri, S., Halekas, J. S., McFadden, J. P., Connerney, J. E. P., Espley, J. R., Harada, Y., et al. (2016). MAVEN observations of partially developed Kelvin-Helmholtz vortices at Mars. *Geophysical Research Letters*, *43*, 4763–4773. https://doi.org/10.1002/2016GL068926

Stergiopoulou, K., Andrews, D. J., Edberg, N. J. T., Halekas, J., Kopf, A., Lester, M., et al. (2020). Mars Express observations of cold plasma structures in the Martian magnetotail. *Journal of Geophysical Research: Space Physics*, *125*, e2020JA028056. https://doi.org/10.1029/2020JA028056

Trotignon, J., Mazelle, C., Bertucci, C., & Acuña, M. (2006). Martian shock and magnetic pile-up boundary positions and shapes determined from the Phobos 2 and Mars Global Surveyor data sets. *Planetary and Space Science*, *54*, 357–369. https://doi.org/10.1016/j.pss.2006.01.003

Xu, Y., Fu, H. S., Liu, C. M., & Wang, T. Y. (2018a). Electron acceleration by dipolarization fronts and magnetic reconnection: A quantitative comparison. *The Astrophysical Journal*, *853*, 11. https://doi.org/10.3847/1538-4357/aa9f2f

Xu, Y., Fu, H. S., Norgren, C., Hwang, K.-J., & Liu, C. M. (2018b). Formation of dipolarization fronts after current sheet thinning. *Physics of Plasmas*, *25*, 072123. https://doi.org/10.1063/1.5030200

Zhang, X., Angelopoulos, V., Artemyev, A. V., & Liu, J. (2018). Whistler and electron firehose instability control of electron distributions in and around dipolarizing flux bundles. *Geophysical Research Letters*, *45*, 9380–9389. https://doi.org/10.1029/2018GL079613

Zhao, M. J., Fu, H. S., Liu, C. M., Chen, Z. Z., Xu, Y., Giles, B. L., & Burch, J. L. (2019). Energy range of electron rolling pin distribution behind dipolarization front. *Geophysical Research Letters*, *46*, 2390–2398. https://doi.org/10.1029/2019GL082100

Zhong, Z. H., Zhou, M., Tang, R. X., Deng, X. H., Turner, D. L., Cohen, I. J., et al. (2020). Direct evidence for electron acceleration within ion-scale flux rope. *Geophysical Research Letters*, *47*, e2019GL085141. https://doi.org/10.1029/2019GL085141